

# Influence of Sidelobes on Fiber-Bragg-Grating-Based $Q$ -switched Fiber Laser

X. P. Cheng, J. Zhang, P. Shum, *Senior Member, IEEE*, M. Tang, and R. F. Wu

**Abstract**—We analyze the influence of sidelobes on fiber-Bragg-grating (FBG)-based  $Q$ -switched fiber laser. Simulation results show the sidelobes of uniform FBG introduce undesired multiple peaks and decrease the output peak power. The experimental results confirm the simulation results.

**Index Terms**—Fiber Bragg grating (FBG), fiber lasers, piezoelectric transducer (PZT) ceramics,  $Q$ -switched lasers.

## I. INTRODUCTION

THE fiber-Bragg-grating (FBG)-based  $Q$ -switched fiber laser (QSFL) is attractive due to its superior all-fiber structure, low loss, good repeatability, and low cost [1], [2]. Reference [3] reported a 18.5-KHz  $Q$ -switched erbium-doped fiber laser (EDFL) using the FBG-based modulator driven by piezoelectric transducer (PZT), and theoretical analyses of the FBG-based  $Q$ -switched EDFL were presented in [4]. However, the Gaussian and super-Gaussian shapes were assumed to be the FBGs' spectra, which neglect the influence of FBGs' sidelobes on  $Q$ -switched pulses performance.

In this letter, we theoretically simulate and analyze the pulses for uniform FBG (UFBG)-based  $Q$ -switched EDFL and compare its counterpart using Gaussian apodized FBG (AFBG). In our simulation, FBGs' spectra with sidelobes in certain bandwidth are considered and integrated into the  $Q$ -switching model. Experiment work under 1-kHz repetition rate was conducted to verify the simulation result. It shows that UFBGs' sidelobes cause multi-peaks of  $Q$ -switched pulses and hence deteriorate the pulses performance. On the other hand, the AFBGs help suppress those multi-peaks, increase the pulses peak power, and improve the  $Q$ -switched pulses performance. To the best of our knowledge, no similar work has been reported in the literatures.

## II. MODELING AND SIMULATIONS

A typical linear cavity FBG-based QSFL laser is shown in Fig. 1. A segment of erbium-doped fiber (EDF) is spliced between two FBGs to form the laser resonator. In this model, FBG1 is fixed, while FBG2 is attached to a PZT and modulated at tunable repetition rate  $f_{\text{rep}}$ . The pump power is coupled

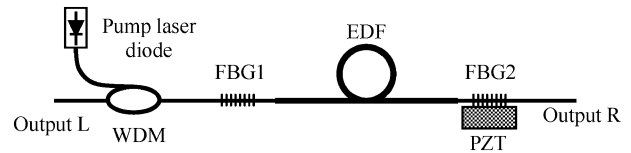


Fig. 1. Configuration of typical FBG-based QSFL.

into the resonator through the wavelength-division-multiplexing (WDM) coupler. The output pulses are extracted through FBGs at both sides of the laser cavity.

The three-level pumping scheme can be used to describe the 1480-nm ( $\lambda_p$ ) pumped EDFL. The population densities in the three energy levels are denoted, respectively, by  $N_1(t, z)$ ,  $N_2(t, z)$ , and  $N_3(t, z)$ , which are functions of time  $t$  and axial position  $z$  in the EDF. We assume that the total erbium ion density  $N_0$  is uniform along the fiber axis. It is also assumed that there is no excited state absorption at  $\lambda_p$ . The pump and signal power are represented by  $P_p^\pm(z)$  and  $P_s^\pm(z)$ , in which the + and - sign denote forward and backward propagating directions. The simplified laser rate equations are given by

$$N_1(z, t) + N_2(z, t) + N_3(z, t) = N_0 \quad (1)$$

$$\frac{\partial N_2}{\partial t} = \frac{\lambda_s}{A_s h c} (\sigma_{sa} N_1 - \sigma_{se} N_2) \cdot (P_s^+ + P_s^-) - \frac{N_2}{\tau_{21}} + \frac{N_3}{\tau_{32}} \quad (2)$$

$$\frac{\partial N_3}{\partial t} = \frac{\lambda_p}{A_p h c} (\sigma_{pa} N_1 - \sigma_{pe} N_3) \cdot (P_p^+ + P_p^-) - \frac{N_3}{\tau_{32}} \quad (3)$$

$$\pm \frac{\partial P_p^\pm}{\partial z} + \frac{1}{v_p} \frac{\partial P_p^\pm}{\partial t} = \frac{b^2}{a_p^2} (\sigma_{pe} N_2 - \sigma_{pa} N_1) P_p^\pm - \alpha_p P_p^\pm \quad (4)$$

$$\pm \frac{\partial P_s^\pm}{\partial z} + \frac{1}{v_s} \frac{\partial P_s^\pm}{\partial t} = \frac{b^2}{a_s^2} (\sigma_{se} N_2 - \sigma_{sa} N_1) P_s^\pm - \alpha_s P_s^\pm + \frac{b^2}{a_s^2} N_2 \sigma_{se} \cdot 2hc^2 \Delta\lambda / \lambda_s^3 \quad (5)$$

In the above equations,  $\tau_{21}$  and  $\tau_{32}$  are the spontaneous lifetime of Level 2 and Level 3 for  $\text{Er}^{3+}$ ,  $\sigma_{sa}$ ,  $\sigma_{se}$ ,  $\sigma_{pa}$ , and  $\sigma_{pe}$  denote the absorption and emission cross sections for signal  $\lambda_s$  and pump  $\lambda_p$ , respectively.  $b$  is the radius of the fiber core,  $A_s$  and  $A_p$  are the mode field area with corresponding radius of  $a_s$  and  $a_p$  for  $\lambda_s$  and  $\lambda_p$ .  $\alpha_s$  and  $\alpha_p$  are the background loss coefficient of  $\lambda_s$  and  $\lambda_p$ . Signal  $\lambda_s$  has a 3-dB bandwidth of  $\Delta\lambda$ ,  $h$  is the Planck's constant,  $c$  is the speed of light in vacuum,

Manuscript received May 11, 2007; revised July 14, 2007.

X. P. Cheng, P. Shum, and M. Tang are with the Network Technology Research Centre, Nanyang Technological University, Singapore 637553, Singapore (e-mail: chen0307@ntu.edu.sg).

J. Zhang is with the Institute of Microelectronics, Singapore 117685, Singapore.

R. F. Wu is with DSO National Laboratories, Singapore 118230, Singapore. Color versions of one or more of the figures in this letter are available online at <http://ieeexplore.ieee.org>.

Digital Object Identifier 10.1109/LPT.2007.904920

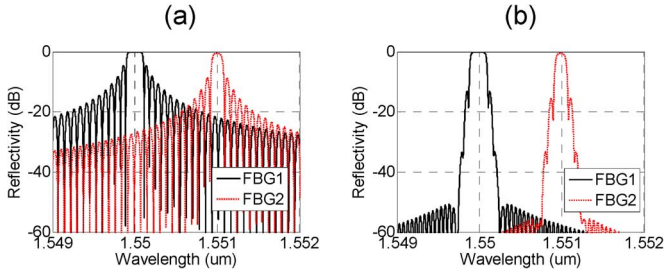


Fig. 2. Reflectivity spectra of UFBGs and AFBGs. (a) UFBG. (b) AFBG.

and  $2hc^2\Delta\lambda/\lambda_s^3$  represents the contribution of the spontaneous emission into  $\lambda_s$ . The boundary conditions are given by

$$\begin{aligned} P_p^+(0, t) &= W_p + R_1(t) \cdot P_p^-(0, t), \\ P_p^-(L, t) &= R_2(t) \cdot P_p^+(L, t) \end{aligned} \quad (6)$$

$$\begin{aligned} P_s^+(0, t) &= R_1(t) \cdot P_s^-(0, t), \\ P_s^-(L, t) &= R_2(t) \cdot P_s^+(L, t). \end{aligned} \quad (7)$$

where  $W_p$  is the pump power at the left end of DCF with length of  $L$ .  $R_1(t)$  and  $R_2(t)$  are the corresponding reflectivity of FBG1 and FBG2 at the oscillation wavelength.

For the FBGs, we calculate the UFBG and AFBG with fourth-order Gaussian shape apodization using the general coupled-mode theory. Their spectra are shown in Fig. 2. Besides the sidelobes, the UFBG pair and AFBG pair have similar characteristics in terms of bandwidth, Bragg wavelength, and peak reflectivity. Their reflectivity spectra are integrated into the boundary conditions (6) and (7). Following that, the steady status of the bidirectional power propagations can be solved iteratively using the Runge–Kutta algorithm. When the PZT is excited periodically by applying modulated voltage, time stepping begins and FBG2's reflectivity spectrum starts to oscillate with applied voltage. It is assumed that the PZT responses linearly during the modulation periods, when the reflectivity spectrum of FBG2 overlaps periodically with that of FBG1. This time-dependent overlapping and the FBGs' wavelength distribution determine the lasing wavelength and the evolution of cavity reflectivity factors ( $R_1(t)R_2(t)$ ). Taking into consideration the time-dependent FBGs' boundary conditions, the coupled rate equations are numerically solved.

In the simulations, 5-m EDF with round-trip time ( $\tau_r$ ) of about 50 ns is adopted.  $\Delta\lambda = 0.1$  nm,  $N_0 = 0.8 \times 10^{-25}$ ,  $\sigma_{21} = 3.8 \times 10^{-25}$  m<sup>2</sup>,  $\sigma_{12} = 3.3 \times 10^{-25}$  m<sup>2</sup>,  $\sigma_{pa} = 1.8 \times 10^{-25}$  m<sup>2</sup>,  $b = 3.5$   $\mu$ m,  $a_s = 3.9$   $\mu$ m,  $\tau_{21} = 10$  ms, and  $\tau_{32} = 7$   $\mu$ s. Pump power  $W_l = 200$  mw. For FBG1, the 3-dB bandwidth is 0.20 nm, peak reflectivity is 99.5%, Bragg wavelength ( $\lambda_{\text{FBG1}}$ ) is 1550 nm, while the PZT driven FBG2 with preapplied tension has a 3-dB bandwidth of 0.12 nm and peak reflectivity of 90.0% at a Bragg wavelength of 1551 nm ( $\lambda_{\text{FBG2}}$ ). When the PZT is excited, the tension is released and FBG2's spectrum moves toward  $\lambda_{\text{FBG1}}$ .

Fig. 3 shows the evolution of cavity reflectivity and oscillation wavelength with minimum round-trip cavity loss ( $(1 - R_1) \times (1 - R_2)$ ) for  $f_{\text{rep}} = 1$  kHz. The graph is plotted against time, which is scaled with respect to  $\tau_r$ . From Fig. 3(c) and (d), we observed that the wavelength evolution has a similar trend for both UFBG and AFBG. When the PZT is excited, the oscillation wavelength starts off from vicinity of  $\lambda_{\text{FBG2}}$  and subsequently moves toward  $\lambda_{\text{FBG1}}$ . When the  $Q$ -switch is turned

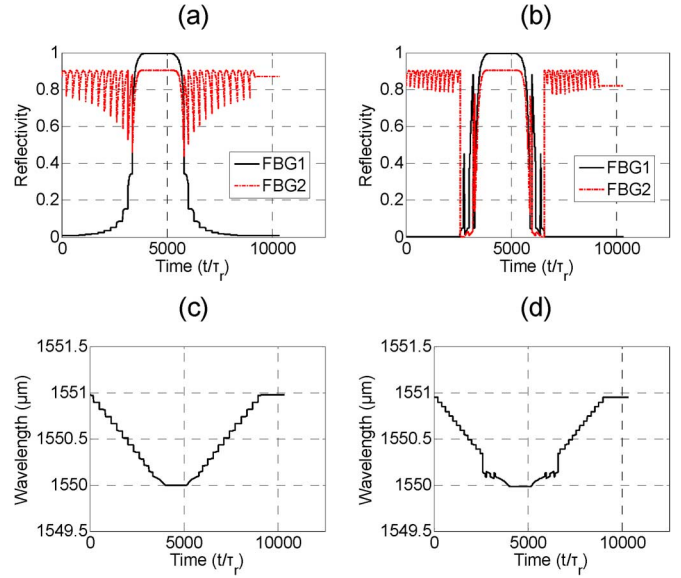
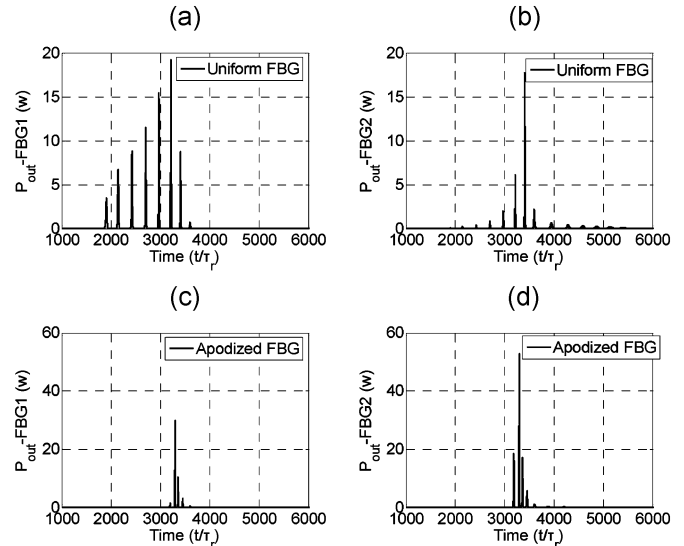

 Fig. 3. Cavity reflectivity and lasing wavelength for UFBG- and AFBG-based  $Q$ -switched EDFL. (a) UFBG. (b) AFBG. (c) UFBG. (d) AFBG.


Fig. 4. Stabilized pulses from both sides of UFBG- and AFBG-based EDFL. (a) Output at FBG1. (b) Output at FBG2. (c) Output at FBG1. (d) Output at FBG2.

OFF, it returns to its initial position. This movement develops step by step with step length depending on the periods of the FBGs' sidelobes. In Fig. 2(b), the AFBGs' spectra have very low reflectivity sidelobes out of the main reflection window. However, on each side of its flat top, there are two sidelobe peaks. As plotted in Fig. 3(b) and (d), these small sidelobe peaks will cause wavelength and the corresponding reflectivity  $R_1$  and  $R_2$  to jitter right before and after fully turning on the  $Q$ -switch.

The output pulses for  $f_{\text{rep}} = 1$  kHz at both ends of the cavity are plotted in Fig. 4. For the UFBG-based EDFL [Fig. 4(a) and 4(b)], we notice that it has very obvious multi-peaks. This undesired multi-peaks output depletes the stored energy in the cavity. On the other hand, it has even higher output power at the left cavity end, which is designed to be the lower output port by using higher reflectivity (99.5%) FBG1. As a result, most energy escapes from FBG1 port and so the output peak power ( $\sim 17.5$  w) at FBG2 port is very low

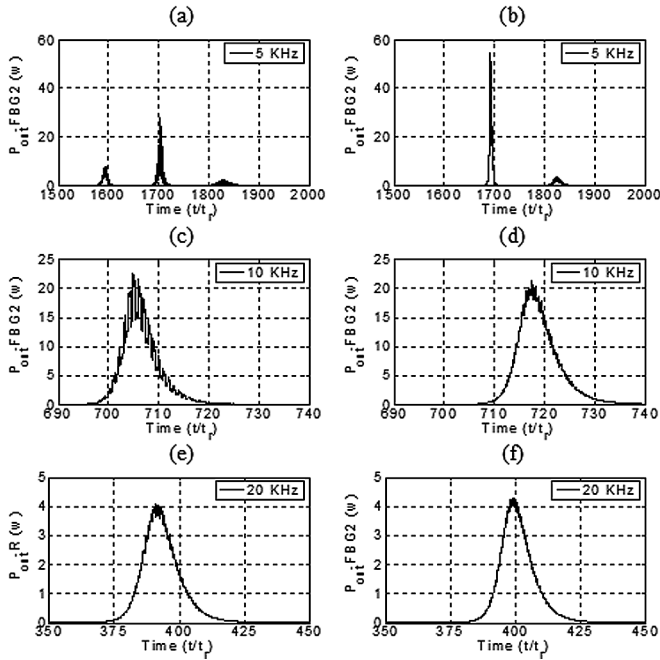


Fig. 5. Output pulses under different repetition rates. (a), (c), (e) UFBG. (b), (d), (f) AFBG.

compared with the peak power ( $>50$  w) of AFBG-based EDFL in Fig. 4(d). Fig. 4(a) and (b) shows us that these undesired multipeak pulses at FBG1 port actually happen earlier than the major pulses lasing out from FBG2. It implies during the modulation period, the relative movements of the sidelobes of both UFBGs interact with each other to result in this multipeak lasing before the  $Q$ -switch is fully turned ON. However, in the case of the AFBG pair, as  $R_1(t)$  is actually very low ( $<30$  dB) out of the  $Q$ -switching opening window [as shown in Fig. 3(b)], the additional pulsing is suppressed effectively.

Fig. 5 shows the output pulses (from FBG2 port) under different repetition rates up to 20 kHz. In this figure, the left column is for UFBG, while the right is for AFBG. Similar to the results for  $f_{\text{rep}} = 1$  kHz, AFBG-based EDFL generates higher output peak power for  $f_{\text{rep}} = 5$  kHz. As  $f_{\text{rep}}$  increases, the peak power approaches a similar level for both UFBG- and AFBG-based EDFLs. This is because under higher repetition rate, the stored cavity energy is rather low, therefore, pulse building up takes a longer time to finish and is, hence, less sensitive to the FBGs' sidelobes as compared to low repetition rate  $Q$ -switching. From the pulses shape, we notice that the envelope of the  $Q$ -switched pulses is much smoother for Gaussian-type AFBG. It argues that the AFBGs with low sidelobes help suppress the multi-peaks, increase the pulses peak power, and improve the FBG-based QSFL performance.

### III. EXPERIMENT RESULTS

For the purpose of experimentally verifying the influence of sidelobes on  $Q$ -switched pulses, both the UFBG and AFBG pairs were fabricated by utilizing a beam-scanning method. All the FBGs' parameters are the same as in the simulation. In our experiment, 1-kHz external pulse waveform was amplified to a certain voltage level and input to the PZT. It periodically tunes the Bragg wavelength of FBG2 within a 1-nm tuning range.

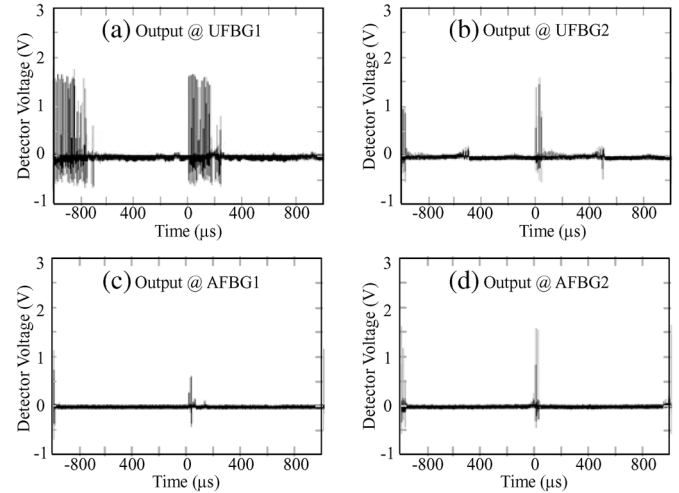


Fig. 6. Experimental results under 1-kHz repetition rate for UFBG- and AFBG-based  $Q$ -switched EDFL. (a) and (b): UFBG. (c) and (d): AFBG.

The output pulses were detected by a low noise photodetector and monitored by Oscilloscope. The results are shown in Fig. 6. The top is for pulses output from UFBG-based EDFL, and the bottom is for AFBG. Comparing the pulses in Fig. 6(a) and (c), it is obvious that the undesired pulses from FBG1 port were suppressed by apodization of FBG. Therefore, we can only observe a few small pulses in Fig. 6(c). It shows a similar result as what we plotted in Fig. 4(c). On the other hand, the output pulses in Fig. 6(d) are much cleaner and have only a few peaks when compared with the result in Fig. 6(b). It verifies the simulation results in Fig. 4 as well. From the above observation, it confirms that AFBGs with low sidelobes help suppress multi-peaks in  $Q$ -switched pulses and eliminate additional power leakage from the undesired output port. It also proves the accuracy of our model of FBG-based QSFL, which involves the FBGs' spectra with sidelobes into the boundary conditions of fiber laser rate equations.

### IV. CONCLUSION

We theoretically simulate the pulses for UFBG-based  $Q$ -switched EDFL, and compare its counterpart under Gaussian-typed AFBGs. In our simulation, FBGs' spectra with sidelobes are calculated and integrated into the QSFL model. Experiment work under 1-kHz repetition rate was conducted to confirm the simulation results. Based on the simulation results and preliminary experimental results, the AFBGs with low sidelobes are strongly recommended for FBG-based QSFL. It will help suppress multi-peaks in  $Q$ -switched pulses, increase the pulse's peak power, and improve the  $Q$ -switched pulse's performance.

### REFERENCES

- [1] J. L. Archambault and S. G. Grubb, "Fiber gratings in lasers and amplifiers," *J. Lightw. Technol.*, vol. 15, no. 8, pp. 1378–1390, Aug. 1997.
- [2] M. J. F. Digonnet, *Rare-Earth-Doped Fiber Lasers and Amplifiers*, 2nd ed. New York: Marcel Dekker, 2001.
- [3] N. A. Russo, R. Duchowicz, J. Mora, J. L. Cruz, and M. V. Andres, "High-efficiency  $Q$ -switched erbium fiber laser using a Bragg grating-based modulator," *Opt. Commun.*, vol. 210, pp. 361–366, 2002.
- [4] R. Duchowicz, N. A. Russo, E. Sicre, and M. V. Andres, " $Q$ -switching of an erbium-doped fibre laser modulated by a Bragg grating fixed to a piezoelectric," *J. Opt. A, Pure Appl. Opt.*, vol. 5, pp. S216–S220, 2003.